ORNL/TM-2020/1469

Report on Partially Complete Post-Irradiation-Examination of the INL Samples

Weicheng Zhong
Lizhen Tan
Oak Ridge National Laboratory

February 28, 2020

OAK RIDGE NATIONAL LABORATORY
MANAGED BY UT-BATTELLE FOR THE US DEPARTMENT OF ENERGY

DOCUMENT AVAILABILITY

Reports produced after January 1, 1996, are generally available free via US Department of Energy (DOE) SciTech Connect.

Website www.osti.gov

Reports produced before January 1, 1996, may be purchased by members of the public from the following source:

National Technical Information Service
5285 Port Royal Road
Springfield, VA 22161
Telephone 703-605-6000 (1-800-553-6847)
TDD 703-487-4639
Fax 703-605-6900
E-mail info@ntis.gov
Website http://classic.ntis.gov/

Reports are available to DOE employees, DOE contractors, Energy Technology Data Exchange representatives, and International Nuclear Information System representatives from the following source:

Office of Scientific and Technical Information
PO Box 62
Oak Ridge, TN 37831
Telephone 865-576-8401
Fax 865-576-5728
E-mail reports@osti.gov
Website http://www.osti.gov/contact.html

This report was prepared as an account of work sponsored by an agency of the United States Government. Neither the United States Government nor any agency thereof, nor any of their employees, makes any warranty, express or implied, or assumes any legal liability or responsibility for the accuracy, completeness, or usefulness of any information, apparatus, product, or process disclosed, or represents that its use would not infringe privately owned rights. Reference herein to any specific commercial product, process, or service by trade name, trademark, manufacturer, or otherwise, does not necessarily constitute or imply its endorsement, recommendation, or favoring by the United States Government or any agency thereof. The views and opinions of authors expressed herein do not necessarily state or reflect those of the United States Government or any agency thereof.

ORNL/TM-2020/1469
M3NA-17OR02040110

FY 2017 Consolidated Innovative Nuclear Research (CINR)
Nuclear Science User Facilities (NSUF)
Light Water Reactor Sustainability (LWRS)

REPORT ON PARTIALLY COMPLETE POST-IRRADIATION EXAMINATION OF THE INL SAMPLES

Weicheng Zhong, and Lizhen Tan
Oak Ridge National Laboratory

Date Published: February 28, 2020

Prepared by
OAK RIDGE NATIONAL LABORATORY
Oak Ridge, TN 37831-6283
managed by
UT-BATTELLE, LLC
for the
US DEPARTMENT OF ENERGY
under contract DE-AC05-00OR22725

CONTENTS

LIST OF TABLES

LIST OF FIGURES

ACKNOWLEDGMENTS

This research was sponsored by the U.S. Department of Energy (DOE), Office of Nuclear Energy (NE), the FY 2017 Consolidated Innovative Nuclear Research (CINR) Nuclear Science User Facilities (NSUF) program and the Light Water Reactor Sustainability (LWRS) program. The authors are grateful to Kory Linton of ORNL and Collin Knight of Idaho National Laboratory for shipping the identified samples and providing essential support on the access to the LAMDA facilities through the NSUF program. We also thank Patricia Tedder, Stephanie Curlin, James Dixon, Brandon Hambrick and Joshua Schmidlin of ORNL for sample reception, preparation, and hardness measurements. T.S. Byun and Omer Karakoc of ORNL are appreciated for technical review of this report.

EXECUTIVE SUMMARY

Ferritic-martensitic steels (NF616 and T91), and austenitic stainless steel 800H and its Grain Boundary Engineering (GBE)-treated version 800H-TMP (ThermoMechanical Processing) were irradiated in the Advanced Test Reactor (ATR) at Idaho National Laboratory (INL) and their microstructures and mechanical properties were characterized. Ferritic-martensitic steels were irradiated up to 8.16 dpa in the irradiation temperatures ranging from 241℃ to 447.5℃. Selected 800H and 800H-TMP samples were also irradiated up to 9.12 dpa at 359℃ to 431℃. Vickers hardness measurement, fractography, and microstructural characterization were performed on the selected samples in the LAMDA lab.

Radiation-induced hardening of NF616 and T91 was observed in the hardness measurements which show ~37% to ~65% increases, depending on irradiation dose and irradiation temperature. Within the irradiation conditions studied in this work, samples with a higher dose had a higher hardness. All the tested alloy 800H and 800H-TMP in this work showed irradiation-hardening by ~96±7% to ~152±10%. Alloy 800H-TMP tended to have slightly smaller irradiation-hardening than alloy 800H.

The fractography of NF616 samples D2 (2.96 dpa at 291.5°C), D4 (5.91 dpa at 359°C), and D6 (8.16 dpa at 431°C) indicated loss of ductility with negligible necking for the sample D2, yet obvious ductile failure for samples D4 and D6. Fractography of alloy 800H samples N4 (7.27 dpa at 359°C), N5 (3.9 dpa at 451.5°C), and N6 (9.01 dpa at 431°C), and alloy 800H-TMP samples P4 (7.36 dpa at 359°C), P5 (3.95 dpa at 451.5°C), and P6 (9.12 dpa at 431°C) indicated that all samples failed in a ductile mode, with obvious necking. Dimples were observed where large Ti-containing particles were observed for the samples.

TEM characterization was performed on alloy 800H (N4, N5, N6) and 800H-TMP (P4, P5 and P6). Accumulation of $M_{23}C_6$ precipitates at grain boundaries was observed in all samples, and the presence of Ti(C,N) precipitates at grain boundaries and in the matrix was observed in alloy 800H-TMP. $M_{23}C_6$ precipitates were found to have the cube-on-cube orientation relationship with the matrix. In addition, nanoscale Si-rich clusters were observed in the matrix of all samples. Atom probe tomography was conducted on the same samples, and their results are being analyzed to be integrated with the TEM results for a confident description of the clustering behavior. Due to the low irradiation temperature (up to 451.5°C), dislocation loops formed in all samples, with the density and the average size of dislocation loops in the order of 10^{22} – 10^{23} m^{-3} and 11.7 – 15.9 nm, respectively. The loop densities in alloy 800H were higher than that in alloy 800H-TMP under the same irradiation conditions.

Further systematic data analyses, together with some complementary experiments, will be pursued for these samples to foster peer-reviewed journal article publications.

1. INTRODUCTION

Advanced alloys are desired to provide greater safety margins, design flexibility and economics compared to the traditional reactor materials. Ferritic-martensitic steel Grade 92 and austenitic Alloy 800/800H are two of the promising alloys interested by the current Advanced Radiation-Resistant Materials (ARRM) and Light Water Reactor Sustainability (LWRS) programs. However, systematic studies on neutron-irradiation induced changes in microstructures and mechanical properties are deficient for those alloys. The objective of this project is to develop correlations between microstructures and mechanical properties of the neutron-irradiated Grade 92 and Alloy 800/800H, based on the experimental results generated from this work. It is expected to develop broader correlations for these types of steels by comparing the results of this work with that of similar alloys such as Grade 91, Alloy 709 and type 304/316 stainless steels from literature and the ongoing studies, with the aid of thermodynamics, kinetics, and microstructural hardening modeling.

Samples of Grade 92 and Alloy 800H selected for this work were irradiated in two test reactors up to ~14 displacements per atom (dpa) at ~241–720°C. The samples of Grade 91, irradiated in the same reactors, were selected as references of Grade 92. Few samples from other two reactors will be included for comparison. Both irradiated and unirradiated samples from the same heat of the materials will be examined to elucidate the radiation-induced evolutions in microstructures, mechanical properties, and deformation mechanisms. To be more specific, mechanical properties such as tensile properties, modulus, hardness, and viscoplasticity will be measured through tensile, Vickers hardness and nanoindentation tests. Microstructural characterization of the samples will be carried out using the state-of-the-art instruments and techniques provided through the Nuclear Science User Facilities (NSUF). The obtained experimental results will then be used to establish the knowledgebase for the effects of alloy chemistry, thermomechanical-processing, and irradiation conditions on microstructures and mechanical properties of Grade 92 and Alloy 800H.

Outcomes of this project will include a comprehensive set of data including microstructures and mechanical properties of both irradiated and unirradiated samples of the interested steels, which will not only help understanding the essential performance of similar alloys, but, more importantly, to gain indispensable insights into the development of advanced alloys with superior radiation resistance. The outcomes can also serve as inputs and/or benchmarks for microstructural and mechanical property modeling of irradiated ferritic-martensitic and austenitic steels. The accomplishment of this project will directly benefit the LWRS program and bring value to the Advanced Reactor Technologies and Small Modular Reactors programs.

The selected samples irradiated in the ATR have been tensile tested and part of samples have been examined. This report summarizes the post-irradiation examination of selected INL samples.

2. SELECTED SAMPLES

A total of twelve INL samples of steels 800H, NF616, and T91 were selected for examination in the study, which were irradiated in the Advanced Test Reactor (ATR) of INL through the University of Wisconsin Pilot Project of the ATR National Scientific User Facility [1]. The steels 800H, NF616, and T91 were commercial heats distributed by INL, Japan Atomic Energy Agency (JAEA), and INL, respectively. The selected samples are listed in Table 1. The samples are in two types - SS-J2 miniature tensile specimen and 3-mm diameter disc.

Table 1. Selected INL samples.

Specimen type	Alloy	Engraved sample code	KGT Num	Temperature (°C)		Dose (dpa)		Dose rate (dpa/s)
				Planned	Average as-run	Planned	As-run total	
Type SS-J2 miniature tensile specimen with 16 × 4 × (<1) mm and gauge 5 × 1.2 × (<1) mm.	800H	N4	1712	400	359	6	7.27	1.30×10^{-7}
		N5	1772	500	451.5	3	3.9	1.35×10^{-7}
		N6	1806	500	431	6	9.01	1.61×10^{-7}
	800H-TMP	P4	2578	400	359	6	7.36	1.31×10^{-7}
		P5	2596	500	451.5	3	3.95	1.37×10^{-7}
		P6	2597	500	431	6	9.12	1.63×10^{-7}
	NF616	D1[*]	402	300	241	3	3.51	1.29×10^{-7}
		D2	1791	300	291.5	6	2.96	5.29×10^{-8}
		D4	1735	400	359	6	5.91	1.06×10^{-7}
		D6	1783	500	431	6	8.16	1.46×10^{-7}
3-mm diameter disc (~0.2-mm thick)	T91	A4	1729	400	447.5	6	4.78	8.51×10^{-8}
		A6	1790	500	429.5	6	7.79	1.39×10^{-7}

[*] The sample D1 is at Argonne National Laboratory (ANL), which is to be in-situ tensile-tested during high-energy x-ray diffraction using the Advanced Photon Source (APS) of ANL.

Other than the standard solution-annealed condition (1177°C for 24 minutes per centimeter of thickness, followed by a water quench) of austenitic stainless steel 800H, the alloy in a thermomechanically processed (TMP) condition, named as 800H-TMP, was irradiated simultaneously. The TMP was constituted of a 6.6 ± 0.2 % thickness reduction by rolling at room temperature, followed by annealing at 1050°C for 90 minutes and water quench, which is a grain boundary engineering (GBE) method to significantly increase the fraction of low-Σ coincidence site lattice (CSL) boundaries, e.g., by nearly 70% (800H-TMP) and ~40% (800H) low-Σ CSL boundaries [2]. GBE with a significantly increased fraction of low-Σ CSL boundaries would benefit a variety of properties such as strength and resistance to creep, stress corrosion cracking, and oxidation [3]. The 800H-TMP exhibited noticeable enhancements in the resistance to thermal aging [4] and corrosion in supercritical water and high-temperature air [5] [6] [7] [8]. Preliminary studies also showed more or less improvements in resistance to neutron irradiation [9] [10]. Therefore, three samples of 800H-TMP, together with three samples of 800H irradiated in nearly identical conditions, were selected in this project to confirm and elucidate the beneficial effects of GBE/TMP on the neutron irradiation resistance of 800H. The other set of samples are ferritic-martensitic steels NF616 and T91, classic/typical versions of Grade 92 and 91, respectively. T91 samples are to be used as reference for NF616.

Each sample was engraved with a unique sample code for visual sample identification and assigned with a unique KGT number for sample library record. The information, together with the planned and as-run irradiation temperature and dose listed in Table 1, was obtained from the material library presented online at https://nsuf.inl.gov. The dose rate in Table 1 was deduced from as-run neutron fluence divided by irradiation time. The irradiation conditions, e.g., temperature and dose, will be compared with the analytical reports of the University of Wisconsin Pilot Project [11] [12] [13].

The compositions of 800H, NF616, and T91 in weight percent (wt%) are listed in Table 2 [1]. These compositions were used for alloy thermodynamic analysis and transmutation analysis to interpret the experimental observations in this project.

Table 2. Compositions in weight percent (wt%) of the INL samples, with Fe as balance[*].

Alloy	Cr	Ni	Mn	Si	Ti	Al	V	W	Mo	Nb	Cu	C	N	P	S
800H/800-TMP	20.42	31.59	0.76	0.13	0.57	0.50					0.42	0.069		0.014	0.001
NF616	8.82	0.174	0.45	0.102		0.005	0.194	1.87	0.468	0.064		0.109	0.0474	0.012	0.0032
T91	8.37	0.21	0.45	0.28		0.022	0.216		0.90	0.076	0.17	0.1	0.048	0.009	0.003

[*] The blank cells are the elements not measured or reported. Oxygen and boron contents were reported as 0.0042% and 0.0017%, respectively, in NF616, which were not reported in the other alloys. 800H was solution-annealed at 1177°C for 24 minutes per centimeter of thickness, followed by a water quench. 800H-TMP was based on 800H, subjected to ~6.6% thickness reduction by rolling at room temperature and then annealed at 1050°C for 1.5 h with water quench. NF616 was normalized at 1070°C for 2 h and tempered at 770°C for 2 h with air cooling. T91 was normalized at 1066°C for 0.8 h and tempered at 790°C for 0.7 h with air cooling.

3. HARDNESS TEST RESULTS

The ATR-irradiated T91, NF616 and 800H/800H-TMP were mechanically polished to a mirror finish for Vickers hardness measurements and microstructural characterization. Vickers hardness measurements were conducted at three levels of loads of 0.1, 0.5, and 1 kgf with three measurements per load. Figure 1a shows the average Vickers hardness with standard deviation for the irradiated NF616 (D2, D4 and D6) and irradiated T91 (A4 and A6). Compared to the Vickers hardness of the unirradiated T91 from literature, which is 210.2 ± 4.2 HV [14], the samples A4 and A6 showed radiation-induced hardening by ~58% and ~65%. The hardness of unirradiated NF616 is 225 HV according to the reference [15], and the samples D2, D4, and D6 show irradiation-hardening of ~37%, ~45%, and ~55%, respectively.

Figure 1b shows the Vickers hardness of unirradiated 800H/800H-TMP, irradiated 800H (N4, N5, N6), and irradiated 800H-TMP (P4, P5, P6). Radiation-hardening was observed for both alloys in all irradiation conditions. The hardness differences among the samples are small considering their standard deviations. Similar to the unirradiated condition, alloy 800H-TMP tended to have slightly higher hardness than alloy 800H in the irradiated conditions. However, the irradiation-hardening of alloy 800H-TMP (e.g., ~96±7% to ~107±11%) tended to be slightly smaller than that of alloy 800H (e.g., ~132±15% to 152±10%).

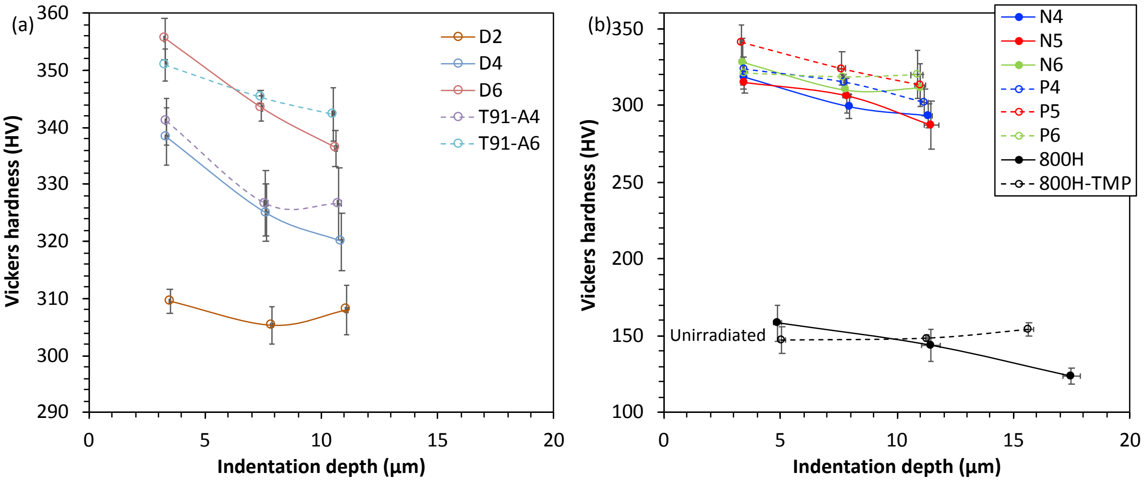

Figure 1. Vickers hardness of (a) NF616 (D2, D4, D6) and T91 (A4 and A6) and (b) alloy 800H (N4, N5, N6) and alloy 800H-TMP (P4, P5, P6) and their corresponding reference.

4. MICROSTRUCTURAL CHARACTERIZATION

Fractography was performed on the fracture surface of the tensile-tested samples using scanning electron microscopy (SEM) and energy dispersive x-ray spectroscopy (EDS) prior to sample polishing. Microstructure of the samples was characterized using transmission electron microscopy (TEM) on electron transparent thin lamellae prepared by focused-ion beam (FIB) for lift-outs from the polished samples.

4.1 FRACTOGRAPHY

Fractography analysis was conducted on the tensile-tested samples of NF616 and 800H and 800H-TMP.

4.1.1 NF616

Figure 2 shows the fractography of the tensile-tested NF616 samples, including D2, D4 and D6. The tensile tests were conducted at room temperature. Sample D2 was irradiated at the lower temperature at 291.5℃, and it showed brittle failure with negligible necking. Cleavage was evident from the fracture surface, where the ‘river-like’ pattern was dominant, as shown in Figure 2d. Samples D4 and D6 were irradiated at higher temperatures at 359℃ and 431℃ respectively, and both samples showed ductile failure mode with obvious necking. Both ‘river-like’ pattern and dimples were observed on the fracture surface of D4, while dimple features were dominant in s the sample D6. Cr-rich particles were observed inside dimples for both D4 and D6, and they were likely Cr-rich $M_{23}C_6$ particles. One of the examples is given in Figure 2f, where $M_{23}C_6$ is marked in the figure. The fractography result was in agreement with the tensile test results, where the sample D2 failed in smaller strain than the samples D4 and D6 in the tensile tests [16].

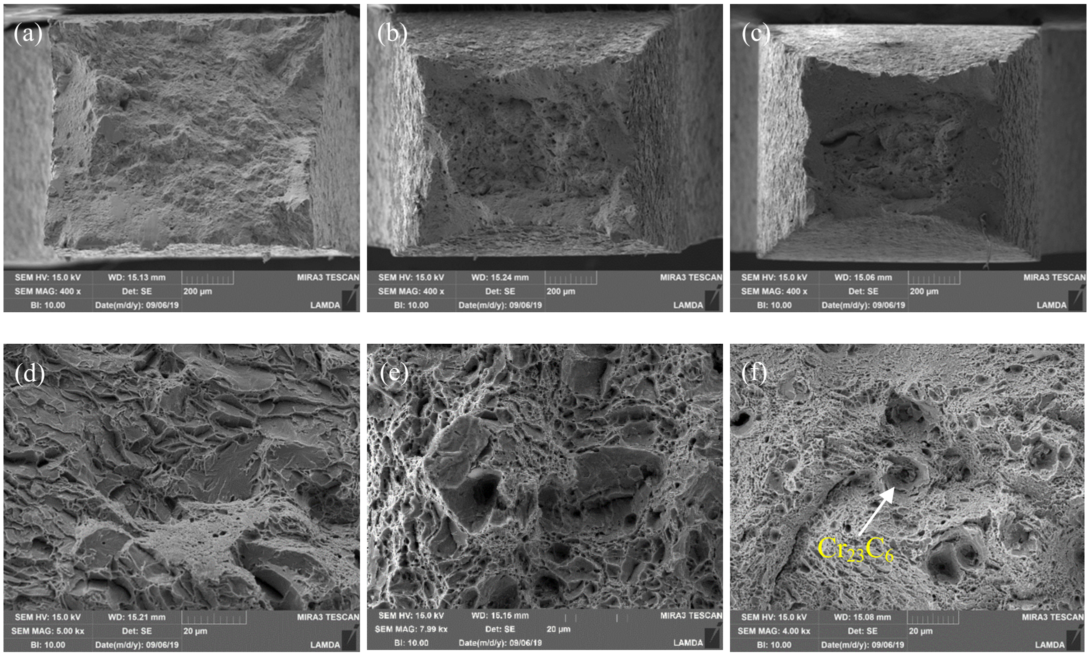

Figure 2. Fractography of the tensile-tested NF616 samples (a, d) D2, (b, e) D4, and (c, f) D6.

4.1.2 800H/800H-TMP

Figure 3 shows the fractography of the tensile-tested N4, N5, N6, P4, P5 and P6. All tested samples failed in ductile mode, where necking was evident. N5 and P5 have lower irradiation doses and higher irradiation temperature than other samples, and necking is more obvious than other samples, indicating samples N5 and P5 could be more ductile than other samples after irradiation. Large Ti-containing particles were observed inside dimples, and the particles had sizes over 5 µm, with two examples of the Tu-containing particles (marked) from sample N5 and P5 shown in Figure 4.

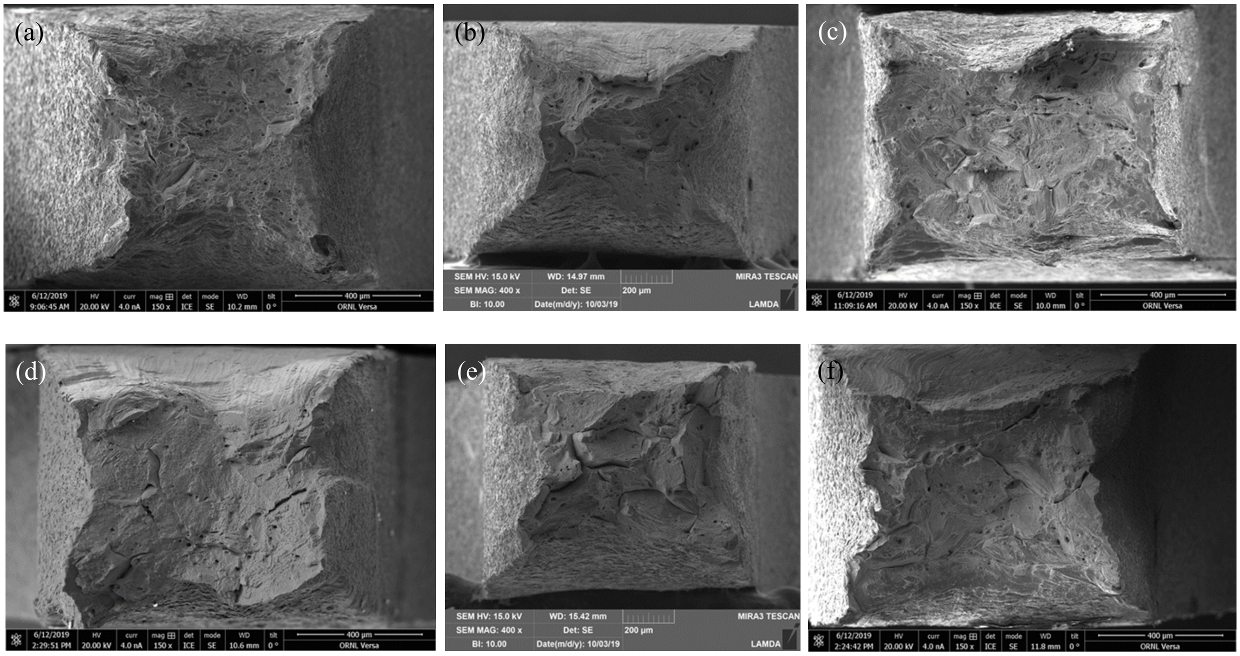

Figure 3. Fractography of the tensile-tested alloy 800H (a) N4, (b) N5, and (c) N6 and alloy 800H-TMP (d) P4, (e) P5, and (f) P6.

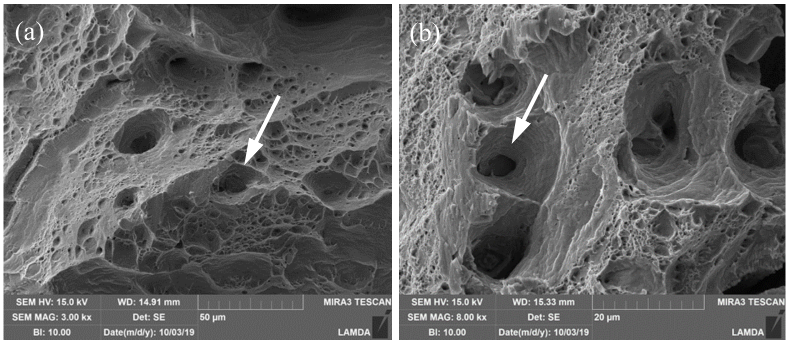

Figure 4. Fractography of tensile-tested (a) alloy 800H N5 and (b) alloy 800H-TMP P5 showing the presence of Ti-containing particles inside dimples.

4.2 TEM RESULTS

4.2.1 800H – N4 (7.27 dpa, 359℃)

Figure 5 shows the microstructure of the tab section of the sample N4. Irradiation induced to form dislocation loops, as shown in TEM dark field image in Figure 5a. The dark field image was taken under the two beam g_{311} near the [011] zone. The diffraction pattern of the two-beam condition is shown in the inset of Figure 5a, with only ¼ dislocation loops were shown in the image. Size distribution of dislocation loops was characterized, and most of the loops had sizes ranging from 5 nm to 15 nm, as shown in Figure 5b. The average size of dislocation loops was measured to be 12.0 ± 5.0 nm. Nanoscale Si rich clusters were observed, as shown in the Si-map in Figure 5.

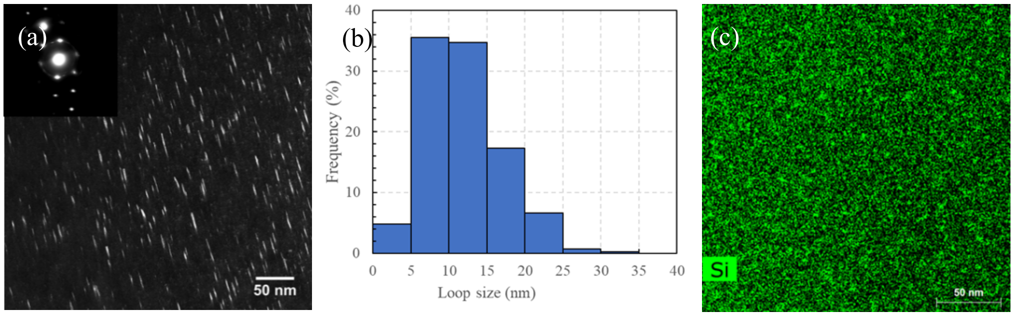

Figure 5. Sample N4: (a) dark field image of dislocation loops, (b) size distribution of dislocation loops, and (c) Si map.

4.2.2 800H-TMP – P4 (7.36 dpa, 359℃)

Figure 6a shows the overview microstructure image of the sample P4. $M_{23}C_6$ (M = primarily Cr) and the Ti(C,N) particles were accumulated at grain boundary, as marked in Figure 6a. Other than at grain boundaries, Ti(C,N) were also distributed in the grain interior with smaller sizes, as shown in the Ti map in Figure 6b. Dislocation loops are shown in Figure 6c, taken under the two-beam g_{113} near the [110] zone. The density of dislocation loops was much lower than that in 800H counterpart (see Figure 5a). The size distribution of dislocation loops is shown in Figure 6d, indicating slightly larger sizes than that in sample N4 (see Figure 5b). The average size was measured to be 15.9 ± 7.2 nm. The Si map shown in Figure 6e indicates the presence of the nanoscale clusters.

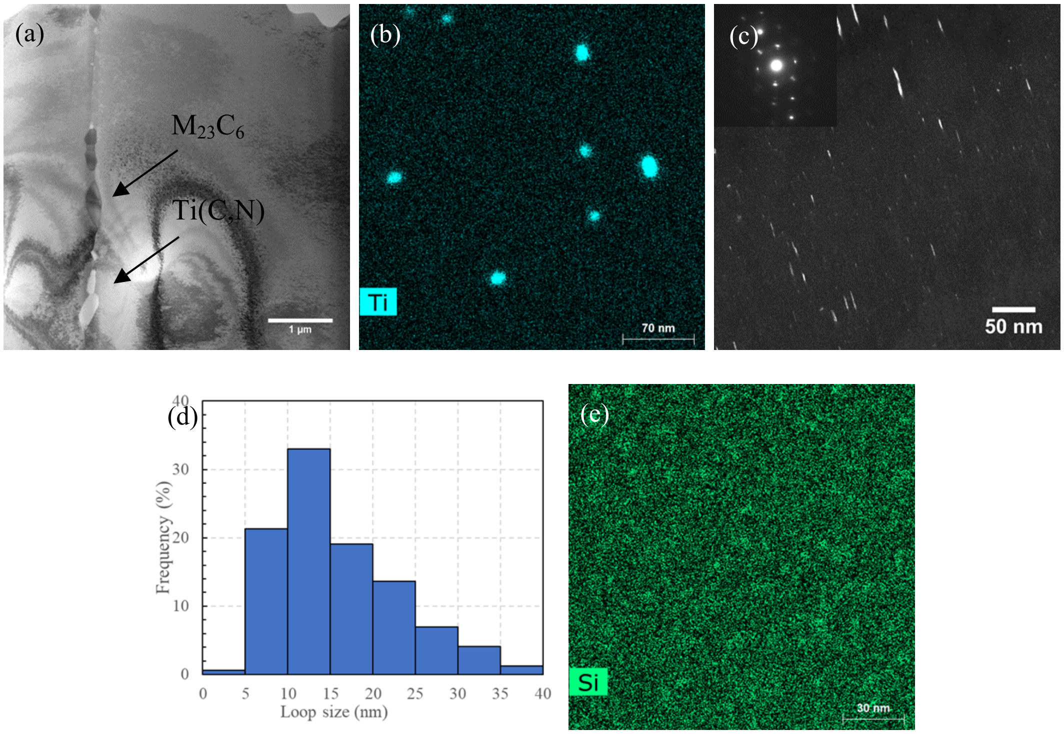

Figure 6. Sample P4: (a) STEM bright field overview image, (b) Ti map, (c) dark field image of dislocation loops, (d) size distributions of dislocation loops, (e) Si map.

4.2.3 800H – N5 (3.9 dpa, 451.5℃)

Figure 7a shows the overview microstructure image of the sample N5, demonstrating that the $M_{23}C_6$ precipitates accumulated at a grain boundary. The dislocation loop image is shown in Figure 7b, which was taken under the two-beam g_{311} near [011] zone as shown in the inset. Size distribution of the dislocation loops was measured and shown in Figure 7c, with the average size of the dislocation loops measured to be 14.1 ± 6.0nm. Nanoscale Si clusters precipitates are present, as shown in the Si map in Figure 7d.

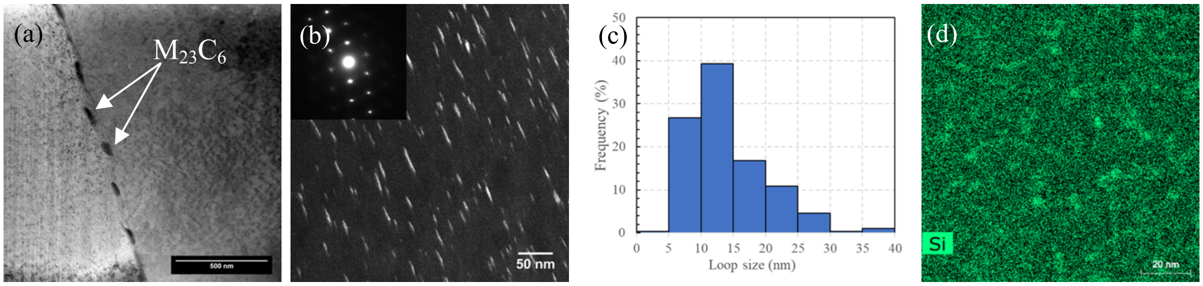

Figure 7. Sample N5: (a) STEM bright field overview image, (b) dark field image of dislocation loops, (c) size distribution of dislocation loops, and (d) Si map.

4.2.4 800H-TMP – P5 (3.95 dpa, 451.5℃)

Figure 8a shows the overview microstructure image of the sample P5. Both $M_{23}C_6$ and Ti(C,N) precipitates were observed at grain boundaries, as marked in the Figure 8a. Small Ti(C,N) precipitates were also observed within the grain, as one of the examples marked. A dislocation loop image is shown in Figure 8b. Again the dislocation loop density in alloy 800H-TMP (sample P5, see Figure 8b) was lower than that in alloy 800H (sample N5, see Figure 7b) with a similar irradiation condition. Size distribution of dislocation loops was measured, as shown in Figure 8c, and the average size of the dislocation loop was 11.7 ± 5.2 nm. The Si map in Figure 8d shows the presence of nanoscale Si clusters in the sample P5, although the contrast is less obvious than that in sample N5 (see Figure 7d).

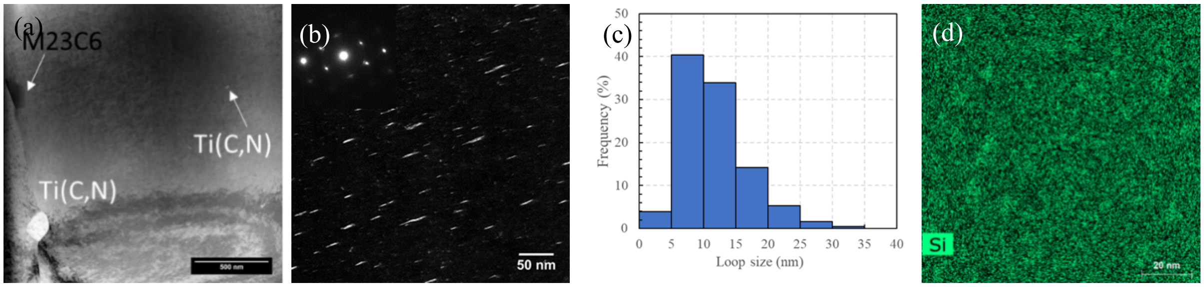

Figure 8. Sample P5: (a) STEM bright field overview image, (b) dark field image of dislocation loops, (c) size distribution of dislocation loops, and (d) Si map.

4.2.5 800H – N6 (9.01 dpa, 431℃)

Figure 9a shows the presence of $M_{23}C_6$ precipitate at grain boundary of the sample N6, and the $M_{23}C_6$ precipitate showed the cube-on-cube orientation relationship with the matrix of the left grain, as the diffraction pattern shown in Figure 9b. Dislocation loops were present, as shown in the Figure 9c. The image was taken under the two-beam condition g_{113} near the [110] zone. Size distribution of dislocation loop is shown in Figure 9d, and the average size of the dislocation loops was measured to be 13.9 ± 6.3nm. the Si map on the Figure 9e shows the presence of Si clusters formation.

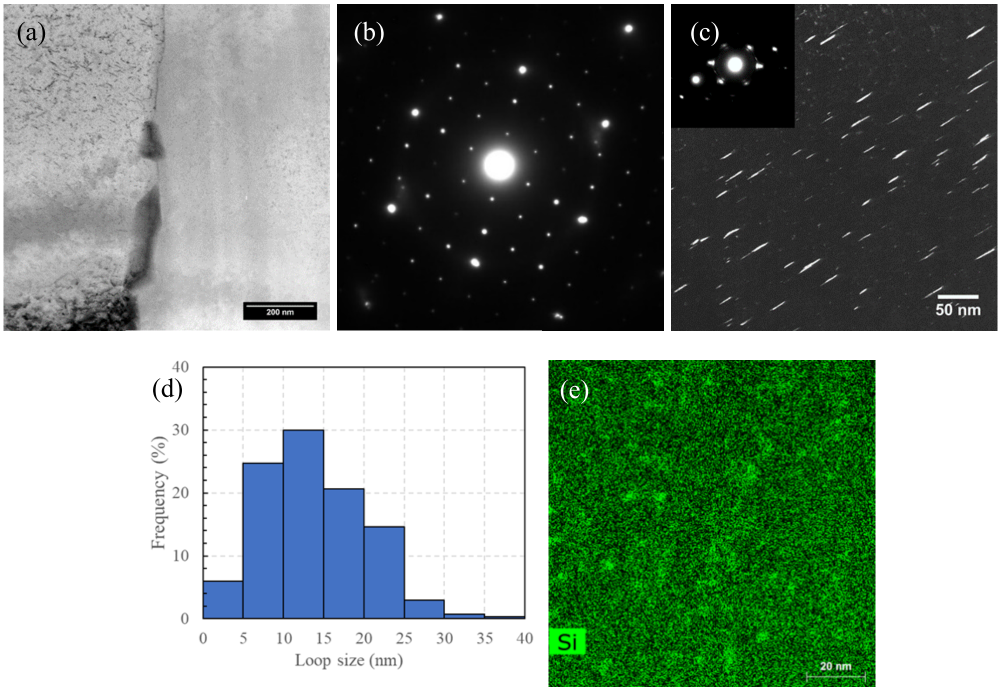

Figure 9. Sample N6: (a) $M_{23}C_6$ precipitate at a grain boundary, (b) diffraction pattern of a $M_{23}C_6$ precipitate with the matrix, (c) dark field image of dislocation loops, (d) size disitrbution of dislocation loops, and (e) Si map.

4.2.6 800H-TMP – P6 (9.12 dpa, 431℃)

Figure 10a shows the overview microstructure image of the sample P6. A high-angle grain boundary and a twin boundary are shown in the Figure. Many $M_{23}C_6$ and Ti(C,N) precipitates were accumulated at the high-angle grain boundary, while only few Ti(C,N) precipitates was observed at the twin boundary. The diffraction pattern of the twin boundary is shown in Figure 10b, which was taken under the [011] zone. Dislocation loops were present, as shown in Figure 10c. Again, the loop density in alloy 800H (Figure 9c) was higher than that in the TMP version (Figure 10c) of same irradiation condition. Figure 10d shows the size distribution of the dislocation loop, and the average size of the dislocation loops was measured to be 13.5 ± 5.7 nm. Si map in Figure 10e shows the presence of Si rich clusters.

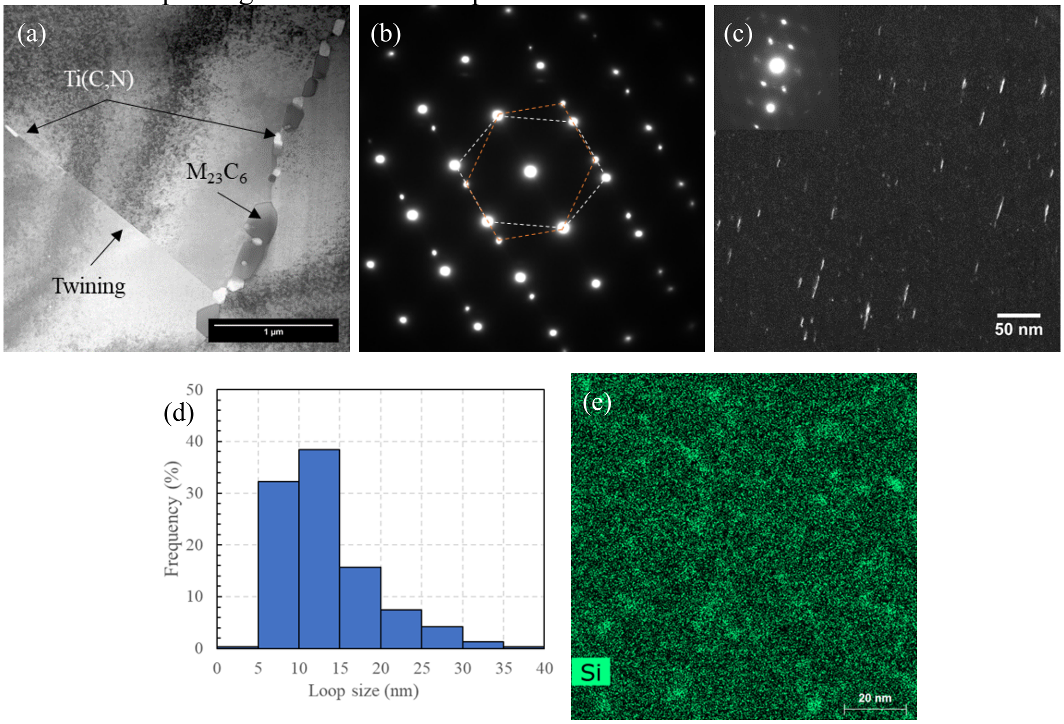

Figure 10. Sample P6: (a) STEM bright field overview image, (b) diffraction pattern of the twin boundary, (c) dark field image of dislocation loops, (d) size distribution of dislocation loops, and (e) Si map.

5. CONCLUSION

Ferritic-martensitic steels (NF616 and T91), and austenitic stainless steel 800H and its Grain Boundary Engineering (GBE)-treated version 800H-TMP (ThermoMechanical Processing) were irradiated in the Advanced Test Reactor (ATR) at Idaho National Laboratory (INL) and their microstructures and mechanical properties were characterized. Ferritic-martensitic steels were irradiated up to 8.16 dpa in the irradiation temperatures ranging from 241℃ to 447.5℃. Selected 800H and 800H-TMP samples were also irradiated up to 9.12 dpa at 359℃ to 431℃. Vickers hardness measurement, fractography, and microstructural characterization were performed on the selected samples in the LAMDA lab.

Radiation-induced hardening of NF616 and T91 was observed in the hardness measurements which show ~37% to ~65% increases, depending on irradiation dose and irradiation temperature. Within the irradiation conditions studied in this work, samples with a higher dose had a higher hardness. All the tested alloy 800H and 800H-TMP in this work showed irradiation-hardening by ~96±7% to ~152±10%. Alloy 800H-TMP tended to have slightly smaller irradiation-hardening than alloy 800H.

The fractography of NF616 samples D2 (2.96 dpa at 291.5°C), D4 (5.91 dpa at 359℃), and D6 (8.16 dpa at 431℃) indicated loss of ductility with negligible necking for the sample D2, yet obvious ductile failure for samples D4 and D6. Fractography of alloy 800H samples N4 (7.27 dpa at 359℃), N5 (3.9 dpa at 451.5℃), and N6 (9.01 dpa at 431℃), and alloy 800H-TMP samples P4 (7.36 dpa at 359℃), P5 (3.95 dpa at 451.5℃), and P6 (9.12 dpa at 431℃) indicated that all samples failed in a ductile mode, with obvious necking. Dimples were observed where large Ti-containing particles were observed for the samples.

TEM characterization was performed on alloy 800H (N4, N5, N6) and 800H-TMP (P4, P5 and P6). Accumulation of $M_{23}C_6$ precipitates at grain boundaries was observed in all samples, and the presence of Ti(C,N) precipitates at grain boundaries and in the matrix was observed in alloy 800H-TMP. $M_{23}C_6$ precipitates were found to have the cube-on-cube orientation relationship with the matrix. In addition, nanoscale Si-rich clusters were observed in the matrix of all samples. Atom probe tomography was conducted on the same samples, and their results are being analyzed to be integrated with the TEM results for a confident description of the clustering behavior. Due to the low irradiation temperature (up to 451.5℃), dislocation loops formed in all samples, with the density and the average size of dislocation loops in the order of $10^{22} – 10^{23}$ m^{-3} and 11.7 – 15.9 nm, respectively. The loop densities in alloy 800H were higher than that in alloy 800H-TMP under the same irradiation conditions.

Further systematic data analyses, together with some complementary experiments, will be pursued for these samples to foster peer-reviewed journal article publications.

6. REFERENCES

[1] H. J. MacLean, K. Sridharan and T. A. Hyde, "Irradiation Test Plan for the ATR National Scientific User Facility-University of Wisconsin Pilot Project," Idaho National Laboratory (INL), 2008.

[2] L. Tan and T. Allen, "An electron backscattered diffraction study of grain boundary-engineered INCOLOY alloy 800H," *Metallurgical and Materials Transactions A,* vol. 36, no. 7, pp. 1921-1925, 2005.

[3] L. Tan, T. Allen and J. Busby, "Grain boundary engineering for structure materials of nuclear reactors," *Journal of Nuclear Materials,* vol. 441, no. 1-3, pp. 661-666, 2013.

[4] L. Tan, L. Rakotojaona, T. R. Allen, R. K. Nanstad and J. T. Busby, "Microstructure optimization of austenitic Alloy 800H (Fe–21Cr–32Ni)," *Materials science and engineering: A,* vol. 528, no. 6, pp. 2755-2761, 2011.

[5] L. Tan, K. Sridharan and T. R. Allen, "The effect of grain boundary engineering on the oxidation behavior of INCOLOY alloy 800H in supercritical water," *Journal of Nuclear Materials,* vol. 348, no. 3, pp. 263-271, 2006.

[6] L. Tan, K. Sridharan and T. R. Allen, "Altering corrosion response via grain boundary engineering," *Materials Science Forum,* vol. 595, pp. 409-418, 2008.

[7] L. Tan, K. Sridharan, T. R. Allen, R. K. Nanstad and D. A. McClintock, "Microstructure tailoring for property improvements by grain boundary engineering," *Journal of Nuclear Materials,* vol. 374, no. 1-2, pp. 270-280, 2008.

[8] L. Tan, T. Allen and Y. Yang, "Corrosion behavior of alloy 800H (Fe–21Cr–32Ni) in supercritical water," *Corrosion Science,* vol. 53, no. 2, pp. 703-711, 2011.

[9] R. K. Nanstad, D. A. McClintock, D. T. Hoelzer, L. Tan and T. R. Allen, "High temperature irradiation effects in selected Generation IV structural alloys," *Journal of Nuclear Materials,* vol. 392, no. 2, pp. 331-340, 2009.

[10] L. Tan, J. T. Busby, H. J. Chichester, K. Sridharan and T. R. Allen, "Thermomechanical treatment for improved neutron irradiation resistance of austenitic alloy (Fe–21Cr–32Ni)," *Journal of Nuclear Materials,* vol. 437, no. 1-3, pp. 70-74, 2013.

[11] K. Davis, J. Rempe, D. Knudson, B. Chase and T. Unruh, "Evaluations of University of Wisconsin Silicon Carbide Temperature Monitors 300 LO and 400 LO B," Idaho National Laboratory (INL), 2011.

[12] S. Wilson, "As-Run Thermal Analysis for the University of Wisconsin Experiment," Engineering Calculations and Analysis Report, 2016.

[13] J. Brookman, "As-Run Physics Analysis for the University of Wisconsin Experiment in the ATR," Engineering Calculations and Analysis Report, 2016.

[14] G. Gupta, Z. Jiao, A. Ham, J. Busby and G. Was, "Microstructural evolution of proton irradiated T91," *Journal of Nuclear Materials,* vol. 351, pp. 162-173, 2006.

[15] J. Jiang, L. Zhu and Y. Wang, "Hardness Variation in P92 Heat-Resistant Steel based on Microstructural Evolution during Creep," *steel research international,* vol. 84, pp. 732-739, 2013.

[16] B. Garrison, W. Zhong, L. Tan and K. Linton, "Tensile Testing and Characterization of Irradiated Grade 92 Ferritic-Martensitic Steels at the IMET Hot Cell and Lambda Facilities," Oak Ridge National Lab.(ORNL), Oak Ridge, TN (United States), 2019.